IEEE Access
Multidisciplinary | Rapid Review | Open Access Journal

Received 23 August 2023, accepted 11 September 2023, date of publication 15 September 2023,
date of current version 25 September 2023.

Digital Object Identifier 10.1109/ACCESS.2023.3315828

RESEARCH ARTICLE

Recoverable Patterning of Macro-Assembled Graphene Nanofilms

XIAOXUE CAO[1,2], JIAHAO LIN[1], SHAOXIONG WU[1], SRIKRISHNA CHANAKYA BODEPUDI[1], (Member, IEEE), ZONGWEN LI[1], FENG TIAN[1], ZHENG LI[1], XINYU LIU[1], LI PENG[1,2], CHAO GAO[2], AND YANG XU[1], (Senior Member, IEEE)

[1]School of Micro-Nano Electronics, ZJU-Hangzhou Global Scientific and Technological Innovation Center, State Key Laboratory of Silicon and Advanced Semiconductor Materials, ZJU-UIUC Joint Institute, Zhejiang University, Hangzhou 310027, China
[2]MOE Key Laboratory of Macromolecular Synthesis and Functionalization, Department of Polymer Science and Engineering, International Research Center for X Polymers, Zhejiang University, Hangzhou 310027, China

Corresponding authors: Li Peng (l-Peng@zju.edu.cn), Chao Gao (chaogao@zju.edu.cn), and Yang Xu (yangxu-isee@zju.edu.cn)

This work was supported in part by the National Natural Science Foundation of China under Grant U22A2076 and Grant 92164106, in part by the National Key Research and Development Program of China under Grant 2022YFA1204304, in part by the China Postdoctoral Science Foundation under Grant 2022T150558, in part by the Natural Science Foundation of Zhejiang Provincial under Grant LDT23F04013F04, in part by the Fundamental Research Funds for the Central Universities under Grant 2021FZZX001-17 and Grant K20200060, and in part by the Zhejiang University (ZJU) Micro-Nano Fabrication Center.

ABSTRACT Patterning is a crucial fabrication step for successfully applying two-dimensional materials in electronic and optoelectronic devices. It can realize miniaturization and help explore new physical phenomena of 2D materials. However, the manufacturing process inevitably introduces defects, which require harsh conditions to recover. Here, we propose a sputtering-lithography-annealing (SLA) strategy for patterning graphene nanofilm with pattern sizes ranging from microns to 100 nm scale without lattice damage. The sputtered masking agents can introduce easily repairable defects into graphene films. Especially, defects introduced by aluminum can be removed entirely. To confirm the validity of the SLA strategy, we prepared macro-assembled graphene nanofilms (nMAG)/Ge and nMAG/Si heterojunction arrays for infrared detection. The patterned detectors present a responsivity of 0.09 A/W at 2 μm (nMAG/Ge) and 26.4 mA/W at 1550 nm (nMAG/Si) with a high array homogeneity, similar to the devices without patterning. This strategy lays the foundation for further exploration of new superstructures of nMAG and can be extended to other 2D materials.

INDEX TERMS Sputter, pattern, macro-assembled graphene nanofilms, nanoribbon recoverable, photodetector.

I. INTRODUCTION

The predicament from Moore's law and the renovation of electronic manufacturing offers the opportunity for two-dimensional (2D) materials with unique geometry [1], [2], [3] and excellent properties [4], [5] to become a compelling candidate for next-generation electronic and optoelectronic devices. Regulating the properties of 2D materials by micro- and nano-fabrication could endow the product with distinct physical properties. For instance, the patterning of 2D materials efficiently improves the transport characteristics of carriers [6], [7], gains more active reaction sites [8], and produces tunable plasmons [9], [10], [11], [12], [13], [14], [15], enhancing the performances of infrared (IR) radiation photodetectors, micro-spectrometers, and biosensors. In addition, the further integration and miniaturization of 2D material-based devices by patterning are of great significance.

Various nano-fabrication schemes and instruments [16], [17], [18], [19], [20], [21], [22], [23], [24] have been used to pattern 2D materials, including bottom-up growth [25], photolithography [18], [26], [27], [28], [29], and laser direct writing [30], [31]. Bottom-up processing strategies could better control the orientation of the nano-structure and rigorously rely on substrates. Complex processes are inevitably accompanied by residues from metal substrates [32] and

The associate editor coordinating the review of this manuscript and approving it for publication was Chi-Tsun Cheng.

transfer agents [33], [34], [35]. Laser-based methods can pattern large-area 2D materials. However, the accuracy is limited to micron order and enormous defects would be introduced at the edges, leading to remarkable performance deterioration [30], [31]. In contrast, traditional lithography methods allow precise control of the shape, size, position, and orientation [36], [37]. Unfortunately, this method is unsuitable for processing 2D materials due to the inevitable introduction of defects in the etching process. An effective protective layer is needed to protect the 2D materials.

Since W. Grove and M. Faraday first observed the phenomenon of sputtering deposits [38], the sputtering technique has been exploited as a compelling film deposition strategy. This technique was widely applied to prepare field-effect transistors (FET) [39], biosensors [40], and photodetectors [41], [42], [43], [44] with the miniaturization and soaring demand of the electronic industry. Compared with other plating strategies, the core competitiveness can be attributed as follows: 1) insensitivity to the deposition temperature; 2) access to deposit compounds like alloy and semi-conductive and insulative films; 3) high deposition efficiency (several seconds/mins) and uniformity [45], [46]. Sputtering has been a vital means of assisting basic research, manufacturing exploitation, and product innovation. However, the incompatibility between the sputtering method and 2D materials hinders further patterning of 2D materials. 2D materials are susceptible to defects introduced by the inevitable high-energy bombard process.

To break through the technical bottleneck and push forward the patterning application of sputtering for 2D materials, we propose a recoverable sputtering-lithography-annealing (SLA) strategy to pattern graphene nanofilm (45 nm-thick) with a minimum feature size of 100 nm on various substrates. We found that the sputtered masking agents can introduce repairable defects into graphene nanofilms. Besides, the influences of annealing conditions, masking agents, and sputtering powers on defect recovery were investigated. The uniform thickness and high surface energy of macro-assembled graphene nanofilms (nMAG) [3], [47], [48], [49], [50], [51], [52], [53], [54], [55] allow us to prepare recoverable nMAG nanoribbons, nMAG/Si, and nMAG/Ge array devices. It is worth noting that the patterned nMAG shows the same lattice structure and photo-thermionic (PTI) emission effect as that of the device made of unpatterned nMAG film. The patterned nMAG-based photodetectors demonstrate high responsivities of 19.16 mA/W at 4 μm (nMAG/Ge) and 1.57 mA/W at 4 μm (nMAG/Si), and high homogeneity). Our SLA strategy solves the incompatibility between 2D materials and sputtering technology and realizes the patterning and miniaturization of bulk 2D materials.

II. MATERIALS AND METHODS

A. CHARACTERIZATION

Raman spectroscopy was performed using a confocal Raman microscope (Senterra, BRUKER) and a Renishaw Invia system with a 532 nm laser. The X-ray photoelectron spectroscopy (XPS) was performed by PHI 5000 C ESCA System operated at 14.0 kV. The XPS of patterned-nMAG by using SLA (Sputter: nMAG after sputtering Al; Sputter + RTP: nMAG after RTP) and photoresist as the protective layer method (ICP: nMAG after ICP; ICP + RTP: nMAG after RTP) were tested to confirm the advantage of SLA strategy. The thickness and morphology of nMAG were investigated by atomic force microscope (AFM, WET-SPM-9500J3). The transmission electron microscopy (TEM) characterization was performed by the Hitachi H-9500 instrument operating at 300 kV. The scanning electron microscopy (SEM) images were obtained on a field-emission SEM system (Hitachi S4800) at an acceleration voltage of 5 kV. The *I-V* curves were measured by Keithley source meter 2450. The IR light was provided by a periodic pulse laser (Light Conversion, OPA-Series, 1 to 10 μm, 200 fs pulse width, and 100 kHz repetition rate).

B. PATTERNING METHOD

We used conventional lithography and rapid thermal processing (RTP) to repair defects of patterned-nMAG (45 nm thickness). First, the nMAG was transferred directly on the germanium substrate with the assistance of tweer and water, forming a clean heterojunction interface with van der Waals contact. Put the sample in a vacuum oven at 60 °C for 24 h to dry out the moisture and enhance the interfacial bonding of nMAG/Ge. For feature size of micrometer, we spin-coated photoresist (AR-5320), then used ultraviolet (UV) lithography to pattern; for nanometer feature size, we spin-coated photoresist (PMMA E-Beam resists AR-P669.04 and AR-P669.03) on the substrate to form an inverted trapezoidal structure, then used the E-Beam lithography (19017898 VOYAGER) to pattern. The magnetron sputtering system (DISCOVERY-635) was used to sputter 40 nm thickness aluminum (Al) on the surface, followed by a lift-off process. Inductively Coupled Plasma Dry Etching System (ICP, OXFORD, Plasmapro100 Cobra 180; ICP_{Power}: 100 W, IF_{Power}: 300 W; Time 3 min; gas: O_2) was used to etch the bare parts. Thenceforth, the Al cladding was removed by immersing into the etching solution (Al and Ag can be removed by H_3PO_4: HNO_3: CH_3COOH: H_2O=73%: 3.1%: 3.3%: 20.6% solution. Silicon oxide can be removed by a buffered oxide etch (BOE).). Finally, we treated the samples by RTP at 500 °C for 1 min to repair the defect introduced during the sputtering process (healing rate: 50 °C/s; cooling rate: 50 °C/min; heat treatment process: 200 °C 5min, 10min, 20 min, 30 min, 40 min; 300 °C 5min, 20 min; 400 °C 2min, 12 min; 500 °C 1min, 2 min, 5 min; 1000 °C 1min, 10 min).

C. DEVICE FABRICATION

We fabricated nMAG/Ge devices using lightly n-doped (10^{15} cm^{-3}) germanium substrate with a thickness of 500 μm. The schematic of the device fabrication is shown in Fig. 1. A 300 nm-thick SiO_2 was grown by plasma-enhanced chemical vapor deposition (PECVD) as an insulating layer after depositing a 2 nm-Al_2O_3 interfacial layer by atomic

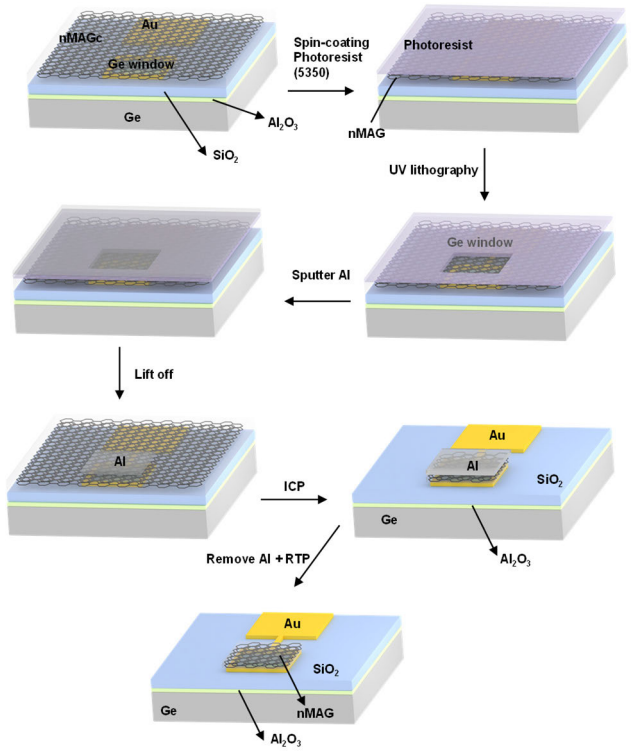

FIGURE 1. The schematic of nMAG/Ge device fabrication.

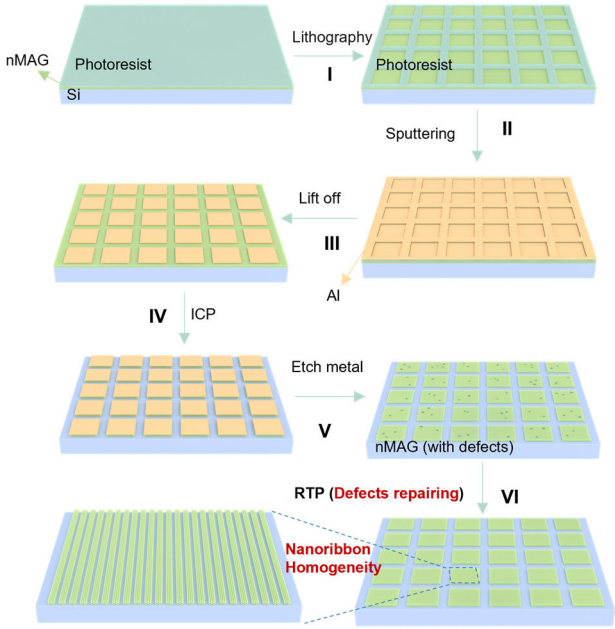

FIGURE 2. The schematic of recoverable patterned-nMAG. This strategy achieves recoverable patterned-nMAG (45 nm-thick) with a minimum size of 100 nm, independent of the 2D material's substrate. It lays the foundation for further exploration of new superstructures of graphene nanofilms and can be extended to other 2D materials.

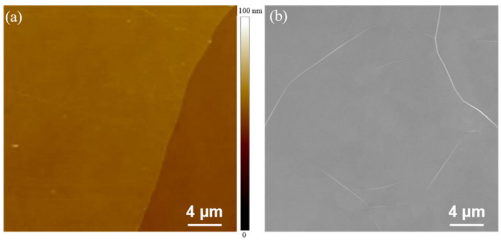

FIGURE 3. AFM (a) and SEM (b) images of nMAG.

layer deposition (ALD). Then, we used lithography (Aligner 12016042 UV) to pattern electrode graphics and sputtered Cr/Au (5/60 nm) on the top layer. After lift-off, the line (1 × 10) array Ge window was patterned with a size of 50 × 50 μm^2 using UV lithography. The nMAG was transferred to the Ge window, where BOE was used to remove the SiO_2 layer. Subsequently, two types of nMAG/Ge devices were fabricated. One was directly transferred on the Ge window; the other was patterned using the strategies described in the patterning method. Finally, GaIn obtained ohmic contact at the back side of Ge, and Au wires were bonded with the top and back electrodes.

The nMAG/Si devices were fabricated using a lightly n-doped (10^{15} cm^{-3}) silicon substrate with a thickness of 500 μm. We used lithography (Aligner 12016042 UV) to pattern electrode graphics and sputtered Cr/Au (5/60 nm) on the top layer. After lift-off, the line (1 × 10) array Si window was patterned with a size of 50 × 50 μm^2 using ultraviolet (UV) lithography. Next, the nMAG was transferred to the Si window, where BOE was used to remove the SiO_2 layer. Subsequently, two types of nMAG/Si devices were fabricated. One was directly transferred on the Si window; the other was patterned using the SLA strategy. Finally, GaIn obtained ohmic contact at the back side of Si, and Au wires were bonded with the top and back electrodes.

III. RESULTS AND DISCUSSIONS

A. PATTERNING STRATEGIES OF NMAG

Fig. 2 illustrates the recoverable patterning strategy of 45 nm-nMAG. The macro- and nano-structures of nMAG were fabricated by lithography (Aligner 12016042 UV for micrometer size; E-Beam lithography for nanometer size). The double-layer photoresist is necessary for this step, forming an inverted trapezoidal structure. This strategy lays the foundation for the lift-off process and nano-structure patterning. Considering the thickness of nMAG, harsh etching parameters are required. Therefore, 40 nm-thick aluminum (Al) was sputtered on the surface of nMAG as a protective layer to avoid the etching of ICP (ICP_{Power}: 100 W; IF_{Power}: 300 W; Time: 3 minutes; gas: O_2). Then the wet etching was used to remove the masking agent. However, the high impact energy of the sputter particles could damage the sp^2 structure of nMAG, thereby deteriorating its lattice structure (II in Fig. 2). Defects caused by physical bombardment are highly recoverable. Here, the low-temperature rapid annealing (RTP < 500 °C) was used to overcome the severe degradation of nMAG by healing the defects.

The wafer-scale nMAG is compatible with the back-end-of-line integration process. The surface tension of water removes most of the wrinkles generated during the transfer

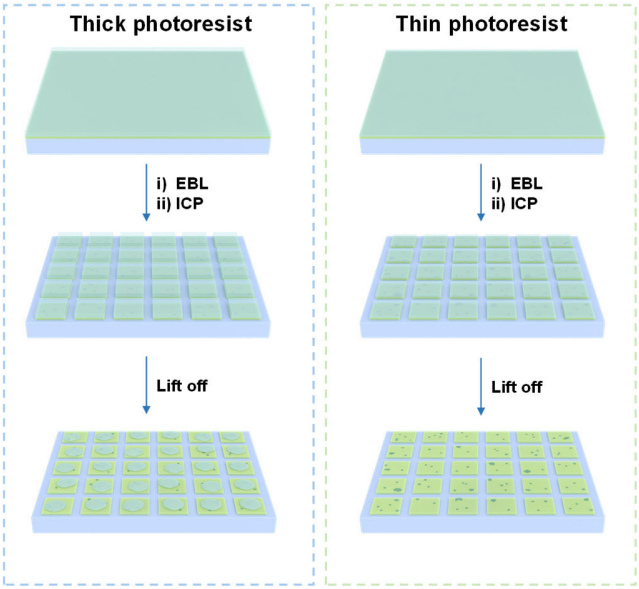

FIGURE 4. The schematic of patterned-MAG by using photoresist as a protective layer.

process. Therefore, the nMAG on silicon shows a flat surface with a few wrinkles, as seen in Fig. 3.

The photoresist was attempted as a protective layer to pattern nMAG (Fig. 4). Considering the thickness of nMAG, a complex etching process is required. To pattern nMAG, a 5 μm thick photoresist (AR-P 5320) is used as a protective layer. The thickness was controlled by the spin-coated conditions (3000rmp, 60s). However, after photolithography, the ICP process results in a cross-linked photoresist structure, as shown by the pink circles in Fig. 5a. Unfortunately, this cross-linked photoresist cannot be removed from the nMAG array surface (marked by green squares).

To effectively remove the residual photoresist, we reduce the thickness of the photoresist to 1 μm (6000rmp, 60s), which efficiently prevents the cross-linking of the photoresist. The clean surface and sharp edges of nMAG in Fig. 5b confirm that the photoresist is removed entirely. However, the photoresist with low thickness cannot effectively protect nMAG from ICP etching. After patterning, the Raman spectrum of nMAG shows a strong D-peak at 1350 cm^{-1} (Fig. 5c). To heal defects and restore the lattice structure of patterned nMAG, a rapid annealing process was performed but failed. Even after a 500 °C treatment for 5 min, an obstinate D-peak (Fig. 5c) is still found. Those results demonstrate that direct photoresist cannot be used for recoverable patterning of nMAG due to the destructive chemical etching of ICP.

Based on the above discussion, we sputtered a masking agent as a protective layer to pattern bulk 2D materials. The patterned-nMAGs with feature sizes ranging from microns (50 μm) to nanometers (100 nm) (Fig. 5d and e) were fabricated using Al as a masking agent. Every step of the SLA patterning strategy (Fig. 2) is depicted by SEM images in Fig. 6. Furthermore, the TEM images illustrate the cross-section of nMAG ribbons with a designed size

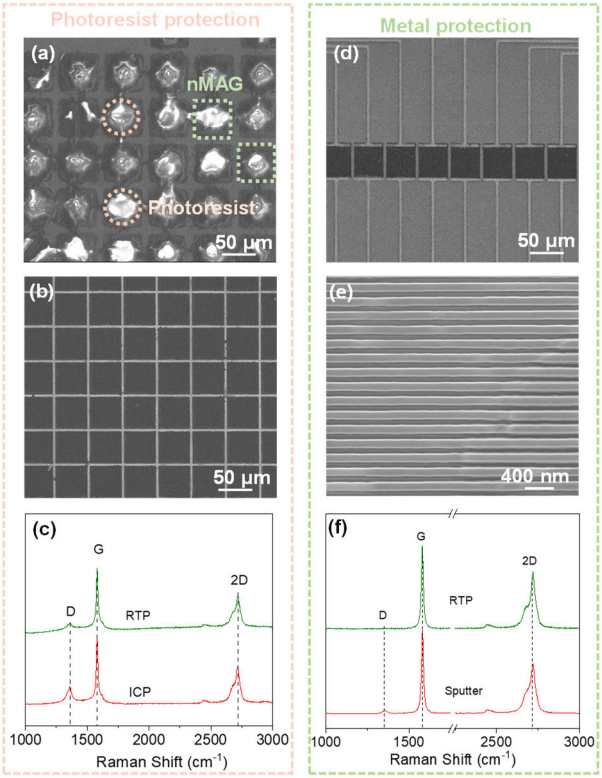

FIGURE 5. Patterning strategies of nMAG. (a) SEM image of patterned-nMAG using a thick photoresist (AR-P 5320, thickness ∼ 5 μm). (b) SEM image of patterned-nMAG using a photoresist (AR-P 5320, thickness ∼ 1 μm). (c) The Raman spectra of nMAG before and after RTP treatment. (d-e) SEM images of patterned-nMAG using an Al masking agent (feature size: 50 μm, 100 nm). (f) The Raman spectra of nMAG before and after RTP (500 °C 5 min) treatment.

of 100 nm before and after patterning (Fig. 7). Besides, the perfect lattice structure in Fig. 7e demonstrates that the patterned nMAG ribbons maintain the same crystallinity with intrinsic nMAG film.

In order to explore the structural evolution during the patterning process, the Raman and XPS were performed. The physical sputtering process will introduce defects to the graphene lattice, evident in the apparent D-peak in the Raman spectrum (Fig. 5f) and sp^3 C peak in the C 1s spectrum of patterned nMAG (Fig. 8b). After 500 °C treatment by RTP, the lattice defects of nMAG introduced by sputtering were rehabilitated, resulting in an undetectable D peak in Raman (Fig. 5f) and sp^3 C peak structure in XPS (Fig. 8b).

The XPS spectra of patterned-nMAGs were measured to analyze the element evolution during the pattering process (Fig. 8). In the sputter and sputter + RTP samples, the negligible O peaks (wide-scan XPS curves, Fig. 8a) and oxygen-free carbon skeletons in the C 1s XPS spectra (Fig. 8b) demonstrate that the trace O comes from the oxygen in the air. After RTP processing (Sputter + RTP), the sp^3 peak at 284.4 eV disappears, indicating the healing of the lattice structure (C sp^2, 284.0 eV) in nMAG.

In the ICP and ICP + RTP cases, the strong D-peak in the Raman spectrum (Fig. 5c), the obvious O peaks (530 eV)

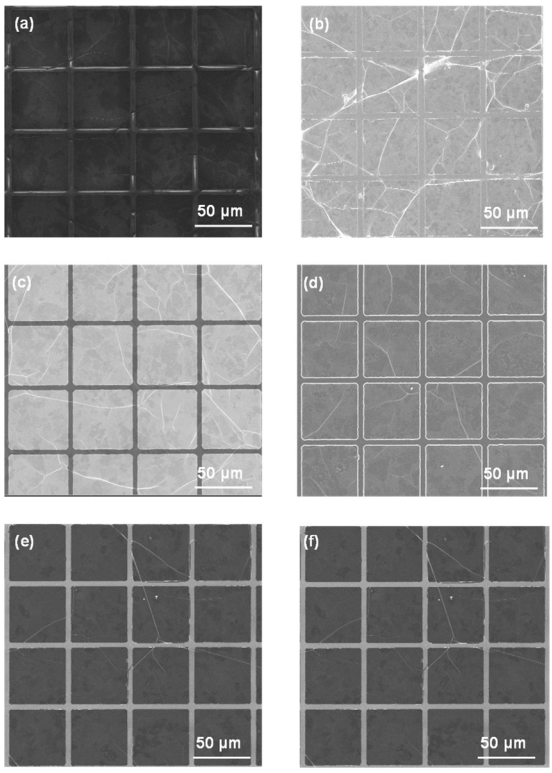

FIGURE 6. The SEM images of patterned-nMAG by using SLA strategy: (a) nMAG with photoresist after UV lithography; (b) nMAG with photoresist after sputtering 40 nm-Al; (c) nMAG with Al after lift-off; (d) patterned-nMAG with Al after ICP; (e) patterned-nMAG after removing Al; (f) patterned-nMAG after RTP.

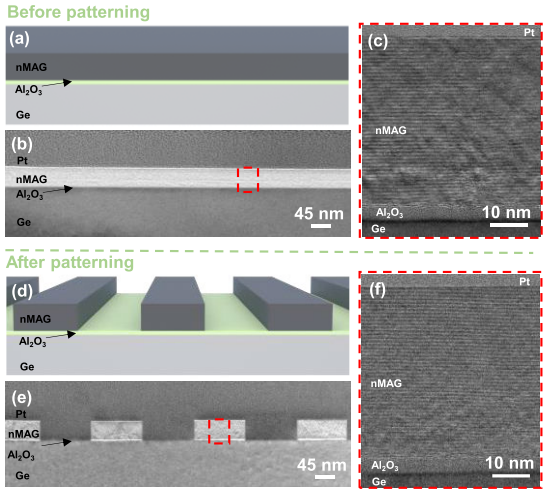

FIGURE 7. (a, d) The schematic of nMAG/Ge before and after patterning. (b-c) TEM images of nMAG/Ge before patterning. (e-f) TEM images of nMAG/Ge after patterning with a feature size of 100 nm.

in the XPS spectrum (Fig. 8a), and complex amorphous carbon skeletons, including C sp^3 (284.4 eV, Fig. 8b), C-O (~285.7 eV, Fig. 8b), C=O (~286.5 eV, Fig. 8b), and COO (~288.1 eV, Fig. 8b), indicate intense oxidation damage of the nMAG lattice during ICP process. After RTP, the intensity of the D peak (Fig. 5c) and O peak (Fig. 8a) decreases due to the partial removal of unstable O-containing functional groups and restoration of lattice defects.

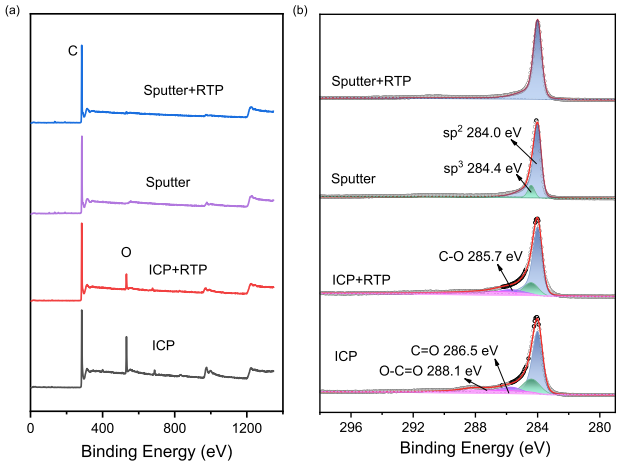

FIGURE 8. (a) The XPS spectra of patterned-nMAG: Sputter: nMAG after sputtering Al by using SLA strategy; Sputter + RTP: nMAG after RTP by using SLA strategy; ICP: nMAG after ICP by using photoresist as the protective layer; ICP + RTP: nMAG after RTP by using photoresist as the protective layer. (b) The C1s XPS spectra of nMAGs patterned by different strategies.

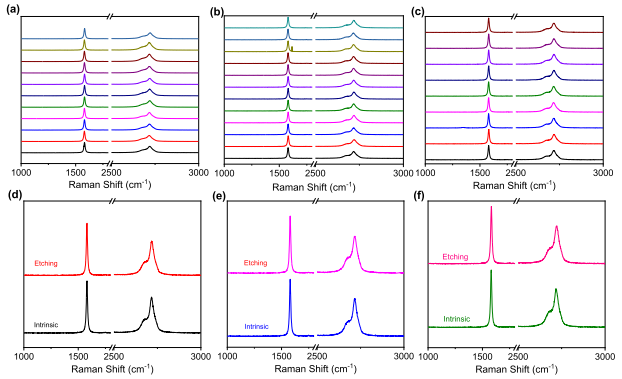

FIGURE 9. (a-c) The Raman spectra of nMAG samples 1-3, which were used for etching by different solutions. Randomly selected points on each sample for Raman testing.The Raman spectra of nMAG before and after etching solution immersion 3 minutes: (d) and (e) H_3PO_4: HNO_3: CH_3COOH: H_2O=73%: 3.1%: 3.3%: 20.6% solution 3 minutes; (f) BOE solution.

B. DEFECTS REPAIRING OF NMAG

To uncover the mechanism of low-temperature defect repair in our protocol, we systematically explored the factors of defect introduction and restoration. To ensure the high quality of the intrinsic sample nMAG, we chose three samples of nMAG. The Raman spectra were measured in different sections on three nMAG samples. The imperceptible D-peak in the Raman spectra indicates a perfect lattice structure of intrinsic nMAG (Fig. 9a-c). The unchanged D peaks of nMAG before and after soaking in different etching solutions (Fig. 9d-e) demonstrate that defects are introduced by sputtering rather than the wet etching process.

To further investigate the relationship between sputtering conditions and defect content of patterned nMAG, the effects of masking agent type, thickness, and sputtering power on the lattice structure were explored. The Raman spectra of sputtered nMAG (Fig. 10a) demonstrate that Al is a better choice of masking agent than Ag and SiO_2 because of the

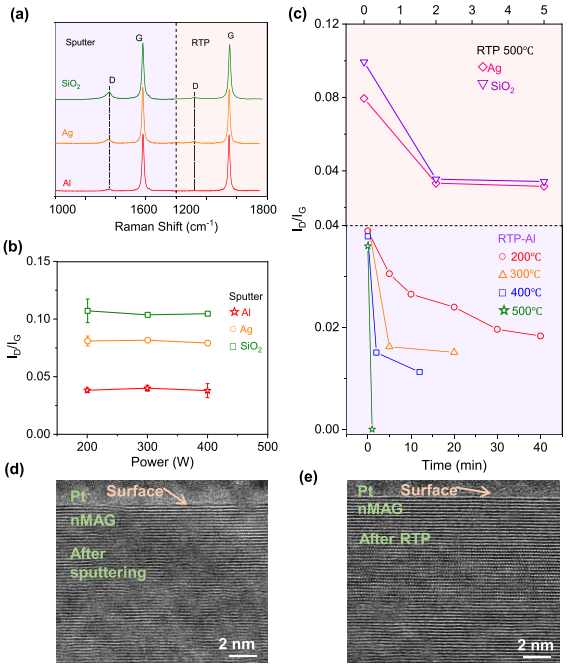

FIGURE 10. Defect repairing of nMAG. (a) The Raman spectra of nMAG sputtered by Al, Ag, SiO_2 and after RTP (Al: 500 °C 1 min; Ag, SiO_2: 500 °C 5 minutes). (b) The I_D/I_G of nMAG sputtered by Al, Ag, and SiO_2 as a function of sputtering power. (c) The I_D/I_G of nMAG sputtered by Al, Ag, and SiO_2 as a function of annealing time under different temperatures. (d-e) Cross-section TEM images of Pt/nMAG after sputtering Al and RTP.

TABLE 1. The values of I_D/I_G (calculated from Fig.11).

Target	Power (W)	I_D/I_G (%)					
40 nm Al	200	3.94	3.99	4.06	4.02		
	300	4.18	3.95	4.12			
	400	4.03	3.76	4.18			
80 nm Al	200	4.12	4.03	4.01			
40 nm Ag		8.27	8.12	8.07	8.01	8.42	
40 nm SiO_2		10.13	10.46	10.29	10.65	10.79	10.66

total healing of defects after RTP. On the one hand, the I_D/I_G value of nMAG sputtered with Al (4%) is half of that sputtered with Ag (8%), far below that of SiO_2 (10%). On the other hand, the defects introduced by Al can be fully healed after 500 °C annealing for 1 min. For nMAGs sputtered by Ag and SiO_2, defect contents are lowered to 3% and 3.5%. The similar intensity of D peaks (Fig. 10b) of nMAGs sputtered by different powers confirms that the defect content of sputtered nMAG is independent of power. The reason is that magnetron sputtering power is related to the number of atoms produced by Ar^+ bombarding the target per unit of time, irrelevant to its energy. Besides, various thicknesses of Al were sputtered on the surface. The target material can act as a protective layer for the nMAG once its surface is completely covered, preventing additional defects caused by the subsequent bombardment of target atoms. The same I_D/I_G values in Raman spectra of nMAGs with different sputtering times verify this observation (Fig. 11 and TABLE 1).

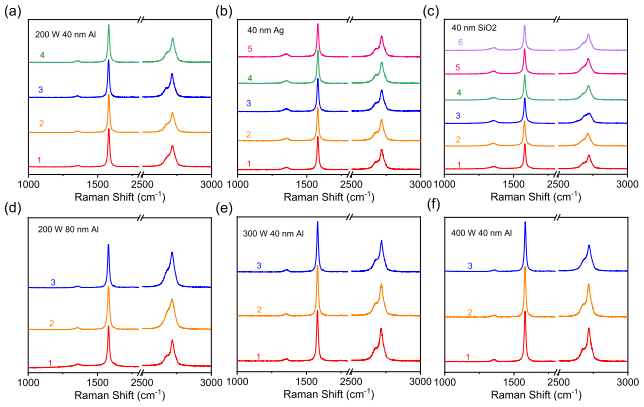

FIGURE 11. The Raman spectra of nMAG sputtered by different power (a, e, f), different targets (a-Al, b-Ag, c- SiO_2), and different thicknesses of (times) masking agents (a, d).

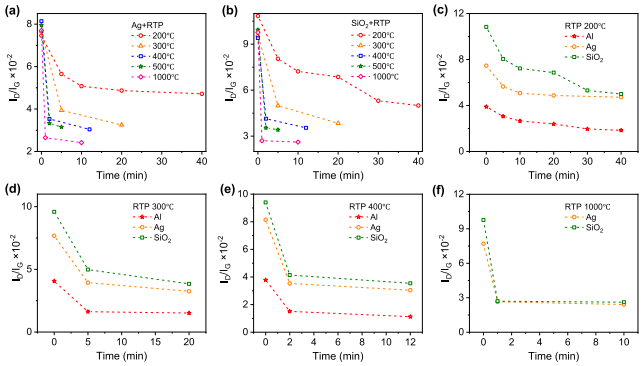

FIGURE 12. The I_D/I_G-T curve of the relationship between defects and annealing time after sputtering Al, Ag, SiO_2.

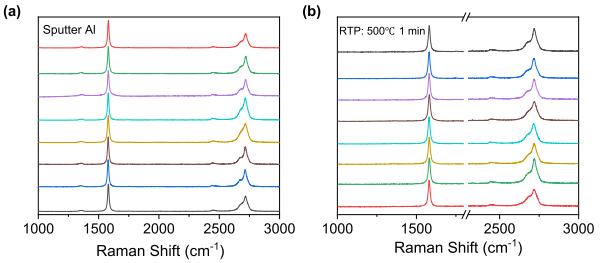

FIGURE 13. The Raman spectral of nMAG after sputtering Al and RTP (8 times repetitions of the experiments, RTP: 500 °C 1 min).

We systematically explored the repairing process of sputtering-induced defects. As discussed above, low-temperature RTP (< 500 °C), a commonly used equipment in device manufacturing, completely repairs the defects introduced by sputtering. The defect recovery results of nMAG are shown in Fig. 10c and Fig. 12. The I_D/I_G values (Fig. 10c) calculated by the semi-in situ Raman spectra of nMAGs sputtered by Al demonstrate that the RTP process could repair the defects under 500 °C for 1 min. For nMAG sputtered with Ag and SiO_2, defect contents are only restored to a minimum of 2.4% after RTP treatment at 1000 °C for 10 minutes (Fig. 13). It is worth noting that the I_D/I_G values decrease rapidly at a specific temperature before stabilizing to a constant value. Besides, defects introduced by sputtering Al as a masking agent can be repaired faster than Ag and

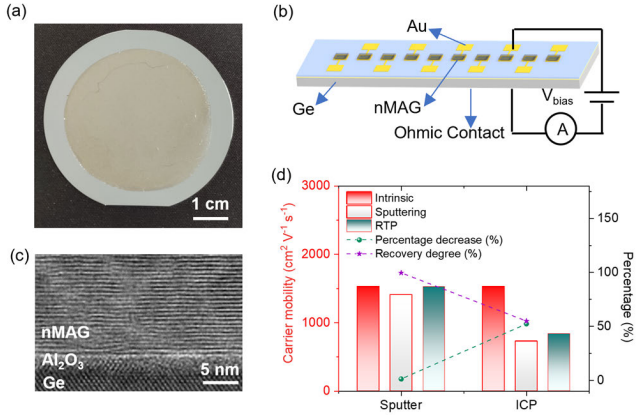

FIGURE 14. Fabrication of nMAG-based array device. (a) The photograph of the nMAG/Ge wafer (2 inches). (b) The schematic of the nMAG/Ge array device. (c)The HR-TEM image of nMAG/Ge. (d) The carrier mobility of nMAG (two methods: sputtering Al as a protective layer and spin-coating photoresist as a protective layer).

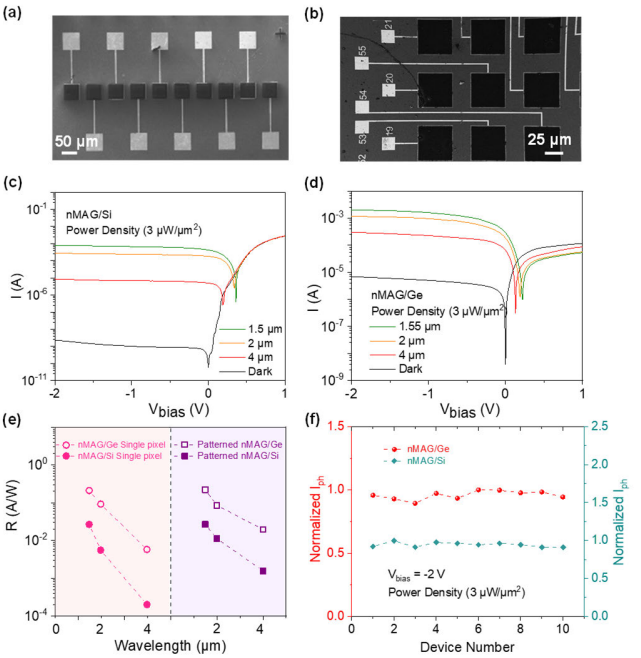

FIGURE 15. Characterization of nMAG-based Array Devices. (a) The SEM image of the nMAG/Ge array device. (b) The SEM image of the nMAG/Si array device. (c-d) The I-V curve of nMAG/Si and nMAG/Ge devices under dark and laser illumination at 1.5 μm, 2 μm and 4 μm wavelength with 3 $\mu W/\mu m^2$ laser power densities (200 fs pulse width, 100 kHz repetition rate). (e) The responsivity of nMAG/Si and nMAG/Ge as a function of wavelength. (f) Uniformity of line array devices under laser illumination at 1550 nm wavelength with 3 $\mu W/\mu m^2$ power density (200 fs pulse width, 100 kHz repetition rate).

SiO_2. Different sputtering targets carry diverse energies resulting in complex defect types [56]. The corresponding threshold temperature is indispensable for defect repair due to the various energy barriers of transformation and migration. The energy of the target atoms produced by Ar^+ bombarding is tightly related to the atomic number of the target. The higher the atomic number of the target, the higher the energy carried by the atoms produced by the Ar^+ bombardment. Furthermore, the energy carried by the target atoms Ar^+ bombardment is not a constant value but has different energy distributions. The number of high-energy atoms produced by Ar^+ bombardment of the Al target is less than that of the Ag target. Therefore, we chose Al as the protective layer. To further verify the recovery of the lattice structure destroyed by sputtering Al, the cross-section TEM images of Pt/nMAG before and after the heat treatment were measured (Fig. 10d-e). The rapid annealing process successfully restores the amorphous graphene lattice of nMAG damaged by sputtering.

To further confirm the reliability of the results of the complete repair of defects by RTP, 8 times repetitions of the repair experiment were measured. Fig. 13a shows the Raman spectra of nMAG after sputtering 40 nm-Al, which show the same I_D/I_G: 4%. Fig. 13b presents the Raman spectra of nMAG after RTP, in which the negligible D peaks proved complete repair of defects. These 8 times repetitions of the repair experiments clearly illustrate that the results are highly reproducible.

C. FABRICATION AND CHARACTERIZATION OF NMAG-BASED ARRAY DEVICE

Recoverable patterning techniques offer opportunities to develop nMAG-based array devices. The wafer-scale preparation (Fig. 14a) of nMAG and van der Waals contacts of nMAG/Ge at an atomic level (HR-TEM cross-sectional image, Fig. 14c) provide the platform for further development of high-performance nMAG/Ge array photodetectors. Based on the benefits of the bulk phase effect of nMAG, nMAG-based infrared detectors have significant prospective applications in infrared detection (Fig. 14d). The carrier mobilities of intrinsic, sputtering, and repairing nMAG are 1530, 1410, and 1524 $cm^2\ V^{-1}\ s^{-1}$, respectively. While in the ICP case, the carrier mobilities of nMAG treated by ICP (photoresist as the protective layer, described in Fig. 5a and d) and repaired nMAG are 730 and 840 $cm^2\ V^{-1}\ s^{-1}$, respectively. Compared with intrinsic nMAG, the carrier mobility of nMAG shows a 52.3% reduction after ICP and a recovery to 54.9% after thermal treatment. These results confirm the advantages of the SLA strategy in patterning 2D materials.

Based on the above discussion, 1 × 10 nMAG/Ge and nMAG/Si array devices were prepared, as depicted in Fig. 15a and b. The schematic of the array device and fabrication are presented in Fig. 14b. The wavelength-dependent temporal photoresponse tests of array devices have been assessed (Fig. 15c and d). Recoverable patterning confers strong photo-thermionic (PTI) emission effects on nMAG-based array devices, leading to high responsivity of 0.21 A/W at 1550 nm, 0.09 A/W at 2 μm and 19.16 mA/W at 4 μm (nMAG/Ge) (Fig. 15e). The responsivity of the nMAG/Si line array device reaches 26.4 mA/W at 1550 nm, 11.2 mA/W at 2 μm, and 1.57 mA/W at 4 μm. The responsivity of the nMAG-based devices before and after patterning (Fig. 15e) is identical at different wavelengths, demonstrating damage-free patterning of 45 nm-nMAG. Furthermore, the

SLA strategy suits various semiconductors. Both nMAG/Ge and nMAG/Si array devices present high homogeneity (Fig. 15f) between individual pixels.

IV. CONCLUSION

We propose a recoverable graphene nanofilm patterning strategy via improved lithography and low-temperature rapid annealing with pattern sizes ranging from micron to 100 nm scale. The repairable process overcomes the technical problem of incompatibility with 2D materials due to the high-energy the sputtering atoms carry. Additionally, masking agent type, thickness, and sputtering power are independent of the defect content of 2D materials. We observed that Al is the best choice for the masking agent than Ag and SiO_2, owing to the lowest defect level after thermal annealing. The high carrier mobility of nMAG ensures superior performance in nMAG-based array devices. The nMAG nanoribbons (45 nm thickness, feature size 100 nm), nMAG/Ge (responsivity of 19.16 mA/W at 4 μm), and nMAG/Si (responsivity of 1.57 mA/W at 4 μm) array devices were prepared using SLA strategy. The patterned-nMAGs demonstrate the same lattice structure and photo-thermionic emission effect as the intrinsic state and high homogeneity. Our strategy is easily adaptable to other bulk 2D material-based devices for patterning and miniaturization.

REFERENCES

[1] L. Tao, Z. Chen, Z. Li, J. Wang, X. Xu, and J. Xu, "Enhancing light-matter interaction in 2D materials by optical micro/nano architectures for high-performance optoelectronic devices," *InfoMat*, vol. 3, no. 1, pp. 36–60, Jan. 2021.

[2] H. Wang, S. Li, R. Ai, H. Huang, L. Shao, and J. Wang, "Plasmonically enabled two-dimensional material-based optoelectronic devices," *Nanoscale*, vol. 12, no. 15, pp. 8095–8108, 2020.

[3] Y. Xu, K. Shehzad, S. C. Bodepudi, A. Imran, and B. Yu, *Graphene for Post-Moore Silicon Optoelectronics*. Hoboken, NJ, USA: Wiley, 2023.

[4] M. Long, P. Wang, H. Fang, and W. Hu, "Progress, challenges, and opportunities for 2D material based photodetectors," *Adv. Funct. Mater.*, vol. 29, no. 19, May 2019, Art. no. 1803807.

[5] J.-H. Kim, J. H. Hwang, J. Suh, S. Tongay, S. Kwon, C. C. Hwang, J. Wu, and J. Young Park, "Work function engineering of single layer graphene by irradiation-induced defects," *Appl. Phys. Lett.*, vol. 103, no. 17, Oct. 2013, Art. no. 171604.

[6] P. Li, D. Collomb, and S. Bending, "High quality hydrogen silsesquioxane encapsulated graphene devices with edge contacts," *Mater. Lett.*, vol. 257, Dec. 2019, Art. no. 126765.

[7] T. Chu and Z. Chen, "Understanding the electrical impact of edge contacts in few-layer graphene," *ACS Nano*, vol. 8, no. 4, pp. 3584–3589, Apr. 2014.

[8] H.-L. Jiang, J. Pan, W. Zhou, H.-M. Li, and S. Liu, "Fabrication and application of arrays related to two-dimensional materials," *Rare Met.*, vol. 41, pp. 262–286, Jan. 2022.

[9] W. A. Murray, S. Astilean, and W. L. Barnes, "Transition from localized surface plasmon resonance to extended surface plasmon-polariton as metallic nanoparticles merge to form a periodic hole array," *Phys. Rev. B, Condens. Matter*, vol. 69, no. 16, Apr. 2004, Art. no. 165407.

[10] P. Zheng, S. K. Cushing, S. Suri, and N. Wu, "Tailoring plasmonic properties of gold nanohole arrays for surface-enhanced Raman scattering," *Phys. Chem. Chem. Phys.*, vol. 17, no. 33, pp. 21211–21219, 2015.

[11] B. M. I. van der Zande, M. R. Böhmer, L. G. J. Fokkink, and C. Schönenberger, "Aqueous gold sols of rod-shaped particles," *J. Phys. Chem. B*, vol. 101, no. 6, pp. 852–854, Feb. 1997.

[12] P. Zheng, S. Kasani, X. Shi, A. E. Boryczka, F. Yang, H. Tang, M. Li, W. Zheng, D. E. Elswick, and N. Wu, "Detection of nitrite with a surface-enhanced Raman scattering sensor based on silver nanopyramid array," *Anal. Chim. Acta*, vol. 1040, pp. 158–165, Dec. 2018.

[13] S. Kasani, P. Zheng, and N. Wu, "Tailoring optical properties of a large-area plasmonic gold nanoring array pattern," *J. Phys. Chem. C*, vol. 122, no. 25, pp. 13443–13449, Jun. 2018.

[14] P. Zheng, H. Tang, B. Liu, S. Kasani, L. Huang, and N. Wu, "Origin of strong and narrow localized surface plasmon resonance of copper nanocubes," *Nano Res.*, vol. 12, no. 1, pp. 63–68, Jan. 2019.

[15] P. Zheng, S. Kasani, and N. Wu, "Converting plasmonic light scattering to confined light absorption and creating plexcitons by coupling a gold nanopyramid array onto a silica–gold film," *Nanosc. Horizons*, vol. 4, no. 2, pp. 516–525, 2019.

[16] J. Lin, O. Cretu, W. Zhou, K. Suenaga, D. Prasai, K. I. Bolotin, N. T. Cuong, M. Otani, S. Okada, A. R. Lupini, J.-C. Idrobo, D. Caudel, A. Burger, N. J. Ghimire, J. Yan, D. G. Mandrus, S. J. Pennycook, and S. T. Pantelides, "Flexible metallic nanowires with self-adaptive contacts to semiconducting transition-metal dichalcogenide monolayers," *Nature Nanotechnol.*, vol. 9, no. 6, pp. 436–442, Jun. 2014.

[17] D. S. Fox, Y. Zhou, P. Maguire, A. O'Neill, C. Ó'Coileáin, R. Gatensby, A. M. Glushenkov, T. Tao, G. S. Duesberg, I. V. Shvets, M. Abid, M. Abid, H.-C. Wu, Y. Chen, J. N. Coleman, J. F. Donegan, and H. Zhang, "Nanopatterning and electrical tuning of MoS_2 layers with a subnanometer helium ion beam," *Nano Lett.*, vol. 15, no. 8, pp. 5307–5313, Aug. 2015.

[18] W.-S. Liao, S. Cheunkar, H. H. Cao, H. R. Bednar, P. S. Weiss, and A. M. Andrews, "Subtractive patterning via chemical lift-off lithography," *Science*, vol. 337, no. 6101, pp. 1517–1521, Sep. 2012.

[19] J. Kim, Y. S. Rim, H. Chen, H. H. Cao, N. Nakatsuka, H. L. Hinton, C. Zhao, A. M. Andrews, Y. Yang, and P. S. Weiss, "Fabrication of high-performance ultrathin In_2O_3 film field-effect transistors and biosensors using chemical lift-off lithography," *ACS Nano*, vol. 9, no. 4, pp. 4572–4582, Apr. 2015.

[20] J. M. Abendroth, N. Nakatsuka, M. Ye, D. Kim, E. E. Fullerton, A. M. Andrews, and P. S. Weiss, "Analyzing spin selectivity in DNA-mediated charge transfer via fluorescence microscopy," *ACS Nano*, vol. 11, no. 7, pp. 7516–7526, Jul. 2017.

[21] X. Xu, Q. Yang, K. M. Cheung, C. Zhao, N. Wattanatorn, J. N. Belling, J. M. Abendroth, L. S. Slaughter, C. A. Mirkin, A. M. Andrews, and P. S. Weiss, "Polymer-pen chemical lift-off lithography," *Nano Lett.*, vol. 17, no. 5, pp. 3302–3311, May 2017.

[22] C. Zhao, X. Xu, Q. Yang, T. Man, S. J. Jonas, J. J. Schwartz, A. M. Andrews, and P. S. Weiss, "Self-collapse lithography," *Nano Lett.*, vol. 17, no. 8, pp. 5035–5042, Aug. 2017.

[23] K. M. Cheung, D. M. Stemer, C. Zhao, T. D. Young, J. N. Belling, A. M. Andrews, and P. S. Weiss, "Chemical lift-off lithography of metal and semiconductor surfaces," *ACS Mater. Lett.*, vol. 2, no. 1, pp. 76–83, Jan. 2020.

[24] G. Yao, D. Zhao, Y. Hong, S. Wu, D. Liu, and M. Qiu, "Direct electron-beam patterning of monolayer MoS_2 with ice," *Nanoscale*, vol. 12, no. 44, pp. 22473–22477, 2020.

[25] S. Wu, D. Zhao, G. Yao, Y. Hong, and M. Qiu, "Lithographic properties of amorphous solid water upon exposure to electrons," *Appl. Surf. Sci.*, vol. 539, Feb. 2021, Art. no. 148265.

[26] Y. Hong, D. Zhao, J. Wang, J. Lu, G. Yao, D. Liu, H. Luo, Q. Li, and M. Qiu, "Solvent-free nanofabrication based on ice-assisted electron-beam lithography," *Nano Lett.*, vol. 20, no. 12, pp. 8841–8846, Dec. 2020.

[27] C. Zhao, X. Xu, S.-H. Bae, Q. Yang, W. Liu, J. N. Belling, K. M. Cheung, Y. S. Rim, Y. Yang, A. M. Andrews, and P. S. Weiss, "Large-area, ultrathin metal-oxide semiconductor nanoribbon arrays fabricated by chemical lift-off lithography," *Nano Lett.*, vol. 18, no. 9, pp. 5590–5595, Sep. 2018.

[28] M. Tu, B. Xia, D. E. Kravchenko, M. L. Tietze, A. J. Cruz, I. Stassen, T. Hauffman, J. Teyssandier, S. De Feyter, Z. Wang, R. A. Fischer, B. Marmiroli, H. Amenitsch, A. Torvisco, M. D. J. Velásquez-Hernández, P. Falcaro, and R. Ameloot, "Direct X-ray and electron-beam lithography of halogenated zeolitic imidazolate frameworks," *Nature Mater.*, vol. 20, no. 1, pp. 93–99, Jan. 2021.

[29] D. Qin, Y. Xia, and G. M. Whitesides, "Soft lithography for micro- and nanoscale patterning," *Nature Protocols*, vol. 5, no. 3, pp. 491–502, Mar. 2010.

[30] P. S. Kollipara, J. Li, and Y. Zheng, "Optical patterning of two-dimensional materials," *Research*, vol. 2020, Jan. 2020, Art. no. 6581250.

[31] A. Castellanos-Gomez, M. Barkelid, A. M. Goossens, V. E. Calado, H. S. J. van der Zant, and G. A. Steele, "Laser-thinning of MoS_2: On demand generation of a single-layer semiconductor," *Nano Lett.*, vol. 12, no. 6, pp. 3187–3192, Jun. 2012.

[32] N. Gao, W. Zhou, X. Jiang, G. Hong, T.-M. Fu, and C. M. Lieber, "General strategy for biodetection in high ionic strength solutions using transistor-based nanoelectronic sensors," *Nano Lett.*, vol. 15, no. 3, pp. 2143–2148, Mar. 2015.
[33] F. Patolsky, G. Zheng, and C. M. Lieber, "Fabrication of silicon nanowire devices for ultrasensitive, label-free, real-time detection of biological and chemical species," *Nature Protocols*, vol. 1, no. 4, pp. 1711–1724, Nov. 2006.
[34] Z. L. Wang and J. Song, "Piezoelectric nanogenerators based on zinc oxide nanowire arrays," *Science*, vol. 312, no. 5771, pp. 242–246, Apr. 2006.
[35] M. Constantinou, G. P. Rigas, F. A. Castro, V. Stolojan, K. F. Hoettges, M. P. Hughes, E. Adkins, B. A. Korgel, and M. Shkunov, "Simultaneous tunable selection and self-assembly of Si nanowires from heterogeneous feedstock," *ACS Nano*, vol. 10, no. 4, pp. 4384–4394, Apr. 2016.
[36] E. Stern, J. F. Klemic, D. A. Routenberg, P. N. Wyrembak, D. B. Turner-Evans, A. D. Hamilton, D. A. LaVan, T. M. Fahmy, and M. A. Reed, "Label-free immunodetection with CMOS-compatible semiconducting nanowires," *Nature*, vol. 445, no. 7127, pp. 519–522, Feb. 2007.
[37] O. Knopfmacher, A. Tarasov, W. Fu, M. Wipf, B. Niesen, M. Calame, and C. Schönenberger, "Nernst limit in dual-gated Si-nanowire FET sensors," *Nano Lett.*, vol. 10, no. 6, pp. 2268–2274, Jun. 2010.
[38] K. Nordlund, S. J. Zinkle, A. E. Sand, F. Granberg, R. S. Averback, R. E. Stoller, T. Suzudo, L. Malerba, F. Banhart, W. J. Weber, F. Willaime, S. L. Dudarev, and D. Simeone, "Primary radiation damage: A review of current understanding and models," *J. Nucl. Mater.*, vol. 512, pp. 450–479, Dec. 2018.
[39] X.-S. Wang, C. Zhou, R. Shi, Q.-Q. Liu, and T.-R. Zhang, "Two-dimensional $Sn_2Ta_2O_7$ nanosheets as efficient visible light-driven photocatalysts for hydrogen evolution," *Rare Met.*, vol. 38, no. 5, pp. 397–403, May 2019.
[40] S. Mao, J. Chang, H. Pu, G. Lu, Q. He, H. Zhang, and J. Chen, "Two-dimensional nanomaterial-based field-effect transistors for chemical and biological sensing," *Chem. Soc. Rev.*, vol. 46, no. 22, pp. 6872–6904, 2017.
[41] P. Yu, Q. Zeng, C. Zhu, L. Zhou, W. Zhao, J. Tong, Z. Liu, and G. Yang, "Ternary Ta_2PdS_6 atomic layers for an ultrahigh broadband photoresponsive phototransistor," *Adv. Mater.*, vol. 33, no. 2, Jan. 2021, Art. no. 2005607.
[42] A. N. Grigorenko, M. Polini, and K. S. Novoselov, "Graphene plasmonics," *Nature Photon.*, vol. 6, no. 11, pp. 749–758, Nov. 2012.
[43] X. Cai, A. B. Sushkov, M. M. Jadidi, L. O. Nyakiti, R. L. Myers-Ward, D. K. Gaskill, T. E. Murphy, M. S. Fuhrer, and H. D. Drew, "Plasmon-enhanced terahertz photodetection in graphene," *Nano Lett.*, vol. 15, no. 7, pp. 4295–4302, Jul. 2015.
[44] M. Freitag, T. Low, W. Zhu, H. Yan, F. Xia, and P. Avouris, "Photocurrent in graphene harnessed by tunable intrinsic plasmons," *Nature Commun.*, vol. 4, no. 1, p. 1951, Jun. 2013.
[45] J. E. Greene, "Review article: Tracing the recorded history of thin-film sputter deposition: From the 1800s to 2017," *J. Vac. Sci. Technol. A, Vac., Surf., Films*, vol. 35, no. 5, Sep. 2017, Art. no. 05C204.
[46] J. T. Gudmundsson, "Physics and technology of magnetron sputtering discharges," *Plasma Sources Sci. Technol.*, vol. 29, no. 11, Nov. 2020, Art. no. 113001.
[47] L. Peng et al., "Multifunctional macroassembled graphene nanofilms with high crystallinity," *Adv. Mater.*, vol. 33, no. 49, Dec. 2021, Art. no. 2104195.
[48] X. Cao, L. Peng, L. Liu, J. Lv, Z. Li, F. Tian, Y. Dong, X. Liu, Y. Shen, H. Sun, Y. Xu, W. Fang, and C. Gao, "Defect-induced photocurrent gain for carbon nanofilm-based broadband infrared photodetector," *Carbon*, vol. 198, pp. 244–251, Oct. 2022.
[49] L. Liu, X. Cao, L. Peng, S. C. Bodepudi, S. Wu, W. Fang, J. Liu, Y. Xiao, X. Wang, Z. Di, R. Cheng, Y. Xu, C. Gao, and B. Yu, "Macroscopic-assembled-graphene nanofilms/germanium broadband photodetectors," in *IEDM Tech. Dig.*, Dec. 2021, pp. 9.2.1–9.2.4.
[50] L. Peng et al., "Macroscopic assembled graphene nanofilms based room temperature ultrafast mid-infrared photodetectors," *InfoMat*, vol. 4, no. 6, Jun. 2022, Art. no. e12309.
[51] W. Liu et al., "Graphene charge-injection photodetectors," *Nature Electron.*, vol. 5, no. 5, pp. 281–288, May 2022.
[52] Y. Dong, J. Lv, J. Chai, F. Tian, X. Cao, X. Liu, L. Chen, S. C. Bodepudi, Y. Zhao, Y. Xu, and B. Yu, "Highly sensitive MoS_2 photodetector based on charge integration and field-coupled effect," *IEEE Trans. Electron Devices*, vol. 69, no. 12, pp. 6884–6889, Dec. 2022.
[53] J. Lv, Y. Dong, X. Cao, X. Liu, L. Li, W. Liu, H. Guo, X. Wang, S. C. Bodepudi, Y. Zhao, Y. Xu, and B. Yu, "Broadband graphene field-effect coupled detectors: From soft X-ray to near-infrared," *IEEE Electron Device Lett.*, vol. 43, no. 6, pp. 902–905, Jun. 2022.
[54] D. Pu, M. A. Anwar, J. Zhou, R. Mao, X. Pan, J. Chai, F. Tian, H. Wang, H. Hu, and Y. Xu, "Enhanced photovoltaic effect in graphene–silicon Schottky junction under mechanical manipulation," *Appl. Phys. Lett.*, vol. 122, no. 4, pp. 1–7, Jan. 2023.
[55] X. Liu, H. Ning, J. Lv, L. Liu, L. Peng, F. Tian, S. C. Bodepudi, X. Wang, X. Cao, Y. Dong, W. Fang, S. Wu, H. Hu, B. Yu, and Y. Xu, "High-performance broadband graphene/silicon/graphene photodetectors: From X-ray to near-infrared," *Appl. Phys. Lett.*, vol. 122, no. 7, Feb. 2023, Art. no. 071105.
[56] X. An, F. Liu, Y. J. Jung, and S. Kar, "Tunable graphene–silicon heterojunctions for ultrasensitive photodetection," *Nano Lett.*, vol. 13, no. 3, pp. 909–916, Mar. 2013.

XIAOXUE CAO is currently pursuing the Ph.D. degree with the Prof. Yang Xu's Laboratory, Zhejiang University, China. Her current research interests include graphene nanofilm preparation and corresponding broadband infrared photodetectors.

JIAHAO LIN received the M.S. degree from the Department of Polymer Science and Engineering, Zhejiang University, China. His current research interests include carbon-based electronics and other advanced devices and applications.

SHAOXIONG WU is currently pursuing the Ph.D. degree with the Prof. Yang Xu's and Hu Huan's Laboratory, Zhejiang University, China. His current research interest includes optoelectronic devices and applications.

SRIKRISHNA CHANAKYA BODEPUDI (Member, IEEE) received the Ph.D. degree from the University of Alberta, Canada. He was a Postdoctoral Fellow with Zhejiang University, where he received the NSFC International Young Scientist's Research Grant. He is currently a Distinguished Researcher with the School of Micro-Nano Electronics, Zhejiang University. He has more than 30 international journal publications, including *Nature Electronics*, *Chemical Reviews*, *Nature Communications*, IEDM, *ACS Nano*, and *Nano Letters*. He coauthored a textbook titled *Graphene for Post-Moore Optoelectronics*. His research interest includes developing low-power, highly efficient broadband image sensors for optical communications and neuromorphic computing. He is an active member of IOP (MInstP). He also serves as the Guest Editor for the Special Issue of *Micromachines*.

ZONGWEN LI is currently pursuing the Ph.D. degree with the Prof. Yang Xu's Laboratory, Zhejiang University, China. He has been working on low-dimensional material-based detectors in materials devices, since 2014. His current research interest includes optoelectronic devices for the broad-spectrum detection of weak signals, such as avalanche photodetectors.

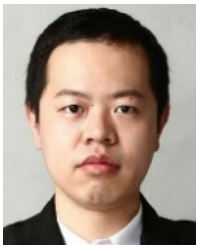

FENG TIAN is currently pursuing the Ph.D. degree with the Prof. Yang Xu's Laboratory, Zhejiang University, China. His current research interest includes optoelectronic devices and applications.

ZHENG LI received the Ph.D. degree in materials science from the Harbin Institute of Technology, China, in 2013. He was a Postdoctoral Fellow with the Group of Prof. Chao Gao, Zhejiang University, China, and a Postdoctoral Fellow with the Group of Prof. Xiaodong Chen, Nanyang Technological University, Singapore. He is currently a PI with the ZJU-Hangzhou Global Scientific and Technology Innovation Center, China. He has published more than 20 international journal publications, including *Science*, *Nature Communications*, *Chemical Reviews*, and *ACS Nano*. His current research interests include the fabrication and functional applications of graphene macro-assembled structures and carbon-based flexible electronics.

XINYU LIU received the B.Sc. degree from Central South University, Changsha, China, in 2018. She is currently pursuing the Ph.D. degree with the Prof. Yang Xu's Laboratory, Zhejiang University, China. Her current research interest includes Si-based 2-D material optoelectronic devices and applications.

LI PENG is currently a Researcher with the Hangzhou International Science and Technology Innovation Center, Zhejiang University. His research interests include preparing, processing, modifying, and functional applying bulk graphene films.

CHAO GAO was a Faculty Member with SJTU, in 2001, and an Associate Professor, in 2002. Since November 2003, he has been with Prof. Sir Harry Kroto as a Visiting Scholar and a Postdoctoral Research Fellow with the University of Sussex, U.K., and then moved to the Prof. Axel H. E. Müller's Group, Bayreuth University, Germany, as an Alexander von Humboldt Research Fellow, in July 2005. He joined the Department of Polymer Science and Engineering, Zhejiang University, and was promoted to Full Professor, in 2008. He co-edited a book on hyperbranched polymers (published by John, Wiley & Sons) and published more than 170 papers with citations of 10000 times and an H-index of 54. His research interests include hyperbranched polymers and graphene. His research on graphene fiber knot was selected by Nature as ''Images of the Year,'' in 2011. He was awarded or funded with the QIAN Baojun Fiber Award Young Scholar, the National Ten-thousand Talents Program, the 2013 Ten Pieces of News in Science and Technology in China, the National Science Fund for Distinguished Young Scholars, the least dense solid Guinness World Records, the ''Gold Kangaroo'' World Innovation Award, the Academician of Asia-Pacific Academy of Materials (APAM), the Zhejiang Youth Technology Award, and the Top 100 National Excellent Doctoral Dissertation of China.

YANG XU (Senior Member, IEEE) received the B.S. degree from the Department of EE, Institute of Microelectronics, Tsinghua University, and the M.S. and Ph.D. degrees in ECE from the University of Illinois at Urbana–Champaign (UIUC), USA. He was a Visiting-by-Fellow of the Churchill College, University of Cambridge, U.K., and a Visiting Professor with the University of California at Los Angles (UCLA). He is currently a Full Professor with the School of Micro-Nano Electronics, Zhejiang University, China. He has published more than 120 articles, including *Nature Electronics*, *Nature Nanotechnology*, *Nature Photonics*, *Chemical Reviews*, *Advanced Materials*, *Nano Letters*, *ACS Nano*, IEEE Electron Device Letters, IEEE Transactions on Electron Devices, IEEE Transactions on Nanotechnology, IEEE Journal of the Electron Devices Society, and IEDM. He authored one Wiley book titled as *Graphene for Post-Moore Silicon Optoelectronics*. He holds over 30 granted patents and has given over 50 talks at international conferences. His current research interests include emerging 2D/3D integrated optoelectronic devices and image sensors for the Internet of Things and post-Moore ubiquitous electronics. He is a fellow of the Institute of Physics (FInstP), a fellow of the Royal Society of Chemistry (FRSC), and a fellow of the Institute of Materials, Minerals and Mining (FIMMM). He is an IEEE EDS Senior Member. He also served as a TPC Member for IEEE EDTM and IEEE IPFA conferences and technical committee of the IEEE EDS Optoelectronic Devices. He is an Editorial Board Member of *Nanotechnology* (IOP) and IEEE Transactions on Electron Devices and an Associate Editor of *Photonics Research* and *Microelectronics Journal*. He is an IEEE NTC Distinguished Lecturer, in 2022 and 2023.